

Accelerating Deep Reinforcement Learning With the Aid of a Partial Model: Power-Efficient Predictive Video Streaming

Dong Liu, Jianyu Zhao, Chenyang Yang, and Lajos Hanzo

Abstract

Predictive power allocation is conceived for power-efficient video streaming over mobile networks using deep reinforcement learning. The goal is to minimize the accumulated energy consumption over a complete video streaming session for a mobile user under the quality of service constraint that avoids video playback interruptions. To handle the continuous state and action spaces, we resort to deep deterministic policy gradient (DDPG) algorithm for solving the formulated problem. In contrast to previous predictive resource policies that first predict future information with historical data and then optimize the policy based on the predicted information, the proposed policy operates in an on-line and end-to-end manner. By judiciously designing the action and state that only depend on slowly-varying average channel gains, the signaling overhead between the edge server and the base stations can be reduced, and the dynamics of the system can be learned effortlessly. To improve the robustness of streaming and accelerate learning, we further exploit the partially known dynamics of the system by integrating the concepts of safer layer, post-decision state, and virtual experience into the basic DDPG algorithm. Our simulation results show that the proposed policies converge to the optimal policy derived based on perfect prediction of the future large-scale channel gains and outperforms the first-predict-then-optimize policy in the presence of prediction errors. By harnessing the partially known model of the system dynamics, the convergence speed can be dramatically improved.

Index Terms

Deep reinforcement learning, energy efficiency, video streaming

I. INTRODUCTION

Mobile video traffic is expected to account for more than 75% of the global mobile data by 2021, and video-on-demand (VoD) services represent the main contributor [2]. Video streaming

D. Liu and L. Hanzo are with the University of Southampton, Southampton SO17 1BJ, UK (email: d.liu, hanzo@soton.ac.uk). J. Zhao and C. Yang are with Beihang University, Beijing 100191, China (e-mail: jianyuzhao_buaa@163.com, cyyang@buaa.edu.cn). This paper was presented in part at IEEE Globecom 2019 [1].

over cellular networks enables mobile users to watch the requested video while downloading [3–5]. To avoid video stalling for a user experiencing hostile channel conditions, a base station (BS) can increase its transmit power for ensuring that the video segment is downloaded before being played. This, however, may cause a significant increase in energy consumption, hence degrading one of the most important design metrics of cellular networks, namely energy efficiency (EE).

The dynamic nature of wireless environment mainly owing to the user behavior, which has long been regarded as being random and remains unexploited in the design of wireless systems. However, with the advent of big data analysis, the user behavior becomes predictable to some degree and hence can be exploited for predictive resource allocation (PRA). For example, by predicting the user trajectory [6] and constructing radio coverage map [7], the future average channel gains in each *time frame*¹ (TF) can be predicted up to a minute-level time horizon. Based on the predicted future channel gains, the BS can transmit more data in advance to the user's buffer during the instances of good channel conditions.

By harnessing various kinds of future information, PRA has been shown to provide a remarkable gain in improving the EE of mobile networks during video streaming [8–13]. Assuming perfectly known future instantaneous channel gains, the trade-off between the required resources and the video stalling duration was investigated in [8]. Assuming perfectly known future instantaneous data rates in each *time slot*² (TS), the total number of TS for video streaming was minimized in [9] to save energy. Considering that future data rates cannot be predicted without errors, the predicted data rate is modeled as random variables with known average values and bounded prediction errors in [10] for optimizing PRA. Since the future data rate of a user depends on the resource allocation, the rate prediction is coupled with PRA and the energy-saving potential of PRA cannot be fully exploited by the policy advocated in [9, 10]. Assuming known future average channel gains, the optimal PRA was derived in [11] for maximizing the EE of video streaming, and was extended to hybrid scenarios, where both real-time and VoD services coexist [14].

To employ these optimized PRA policies, an immediate approach is to first predict the future information by machine learning and then allocate resource by solving optimization problems

¹In this paper, a time frame refers to the duration of time, say one second, where the large-scale channel gain can be regarded as a constant, instead of the “video frames” that compose a video segment.

²A time slot typically has a duration of milliseconds within the channel's coherence time, where the small-scale fading can be regarded as a constant.

based on the predicted information [12, 13]. Such an approach is operated in four phases. The first phase represents training a predictor (say for predicting the future average channel gains) in an off-line manner using historical data [6]. The second phase corresponds to gathering data (say the locations along the user trajectory) for making a prediction after a user initiates a request. The third phase assigns radio resources to all the TFs or TSs in a prediction window at the start of the window. Finally, the BS allocates resources and transmits to the user in each TS according to the pre-assigned resources. When a user starts to play a video file, a central unit in the network has to gather data for making a prediction. Before future resources have been allocated with the predicted information, however, the BS has to serve the user in a non-predictive manner. Furthermore, the first-predict-then-optimize procedure is tedious, and the resultant PRA policy cannot be accurately matched to the dynamically fluctuating wireless environment. Furthermore, the prediction accuracy degrades as the prediction horizon increases. A natural question is: can we optimize PRA in an on-line and end-to-end manner?

Reinforcement learning (RL) [15] can be invoked for on-line learning by interacting with dynamic environments. Recently, deep learning [16] has been introduced as a breakthrough solution, heralding a new era for RL, namely deep reinforcement learning (DRL), which relies on the powerful family of deep neural networks (DNNs). With the aid of the new paradigm of mobile edge computing (MEC) [17], DRL becomes capable of addressing various challenging problems [18–21]. Yet, standard DRL algorithms are designed for dealing with entirely model-free tasks, whose convergence speed may still be unsatisfactory even upon adopting DNNs. Fortunately, for many wireless problems, a part of the dynamic model is known. Nevertheless, how to exploit such knowledge for accelerating DRL is an open question at the time of writing.

Against this background, we propose a DRL framework for optimizing predictive power allocation and illustrate how to accelerate DRL with the aid of a partial model. We consider a scenario where users travel across multiple cells covered by a MEC server during video streaming. The objective is to minimize the total average energy consumed for streaming under the throughput constraint that avoids video stalling. We formulate a Markov decision process (MDP) by judiciously designing the *action* and *state*, so that the policy can exploit the dynamics of the system without explicit prediction, whilst imposing a significantly reduced signaling overhead. To cope with the continuous nature of the state and action spaces, we rely on the deep deterministic policy gradient (DDPG) [22] to solve the MDP. To improve the robustness and accelerate the learning procedure, we tailor the basic DDPG algorithm for exploiting the partially

known dynamics, by integrating the concepts of safe layer, post-decision state (PDS) and virtual experiences introduced in [23, 24]. Our simulation results show that the proposed DRL-based policies converge to the optimal policy derived based on perfect future channel prediction and achieve lower energy consumption compared with the optimal PRA in the presence of prediction errors. By exploiting the partial knowledge on the dynamics, the interactions between agent and environment can be significantly reduced. Our major contributions are summarized as follows:

- Instead of directly regarding the transmit power in each TS as the action of the RL agent, we first derive the optimal power allocation policy in closed-form for an arbitrary given average data rate in each TF by exploiting the knowledge on the distribution of small-scale fading. In this way, we can set the average data rate as the action without loss of optimality, and hence the system's state only depends on the slowly-varying average channel gains. This avoids millisecond-level information exchange between the MEC server and BSs, and makes it easier for the agent to learn the dynamics of the system.
- Inspired by the idea of safe RL designed for the situations where the safety of the agent (say a robot) is particularly important [23], we design a safe layer for the actor network in DDPG for satisfying the throughput constraint. This avoids introducing a penalty term in the reward function, eliminates a hyper-parameter that requires sophisticated tuning, and hence improves the robustness of the policy learned. In contrast to [23] that is designed for completely unknown environments, the safe layer in this work is derived in closed-form by exploiting the system's partially known dynamics.
- Inspired by the idea of introducing PDS to accelerate Q-learning by dividing the system's dynamics into known and unknown components [24], we integrate PDS into DDPG and propose the amalgamated PDS-DDPG algorithm, which significantly reduces the number of unknown parameters in the DNNs. In contrast to [24], the proposed PDS-DDPG algorithm beneficially harnesses DNNs and it becomes eminently suitable for learning in continuous state and action spaces.
- We further exploit the property that the unknown dynamics are independent of the known dynamics by generating virtual experiences based on historical data. By training relying on both virtual and real experiences, the convergence speed can be dramatically boosted.
- Our technique of integrating the PDS, safe layer and virtual experience into DRL is applicable to numerous wireless tasks for accelerate RL by exploiting a partial model on the

system dynamics, provided that certain properties are satisfied.

The rest of the paper is organized as follows. In Section II, we introduce the system model. In Section III, we formulate the RL problem and solve it using DDPG. In Section IV, we exploit the partially known dynamics by integrating the concepts of safer layer, PDS and virtual experience into the basic DDPG. Our simulations results are provided in Section V, and finally, Section VI concludes the paper.

II. SYSTEM MODEL

We consider a learning-aided network architecture [25] relying on MEC as shown in Fig. 1, where the BSs in an area are connected to a MEC server. The MEC server monitors and records the status of mobile users (say the channel conditions and buffer status) and BSs (say the consumed energy), which are then sent to the cloud server and stored in the database as training samples. A centralized learner within the cloud server learns the transmission policy based on the training samples stored in the database, and issues the learned policy to the MEC servers. Each MEC server stores the learned policy, based on which the MEC server sends instructions to the BSs to implement the transmission policy.

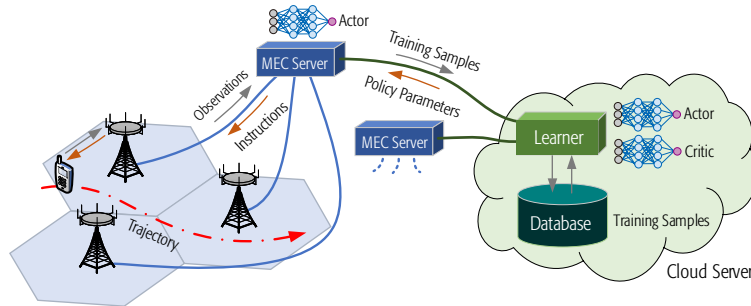


Fig. 1. Learning-aided cellular network architecture.

Each user requesting a video file from the content sever may travel across multiple cells during the video streaming process. We assume that each user is associated with the BS with the strongest average channel gain, and each BS serves the associated users over orthogonal time-frequency resources. Since all the users in the considered network share the same network topology (e.g., BS locations), system configurations (e.g., maximal transmit power and transmission bandwidth), wireless channels (e.g., path loss and small-scaling fading distribution), and road topology, we consider a randomly chosen user and the learned policy is applicable to every user.

A. Transmission and Channel Models

Each video file is partitioned into N_v segments, each of which is the minimal unit for video playback. The playback duration of each segment is further partitioned into L_v TFs, each with duration ΔT . Each TF is divided into N_s TSs, each having a duration of τ , i.e., $\tau = \Delta T/N_s$, as shown in Fig. 2. The large-scale channel gains (i.e., average channel gains) are assumed to remain constant within each TF, but naturally, it may change from one TF to another due to user mobility. The small-scale channel gains are assumed to remain constant within each TS, but they are independently and identically distributed (i.i.d.) among TSs.

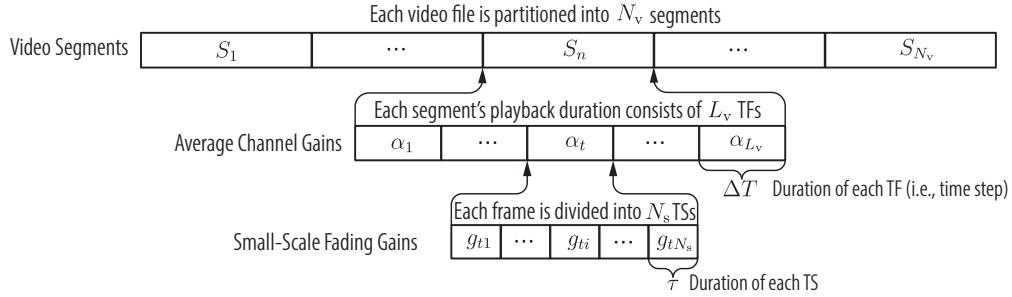


Fig. 2. Video segment playback duration and channel variation.

Let $\alpha_t g_{ti}$ denote the instantaneous channel gain between a user and its associated BS in the i th TS of the t th TF, where α_t and g_{ti} denote the large-scale channel gain and the small-scale fading gain, respectively. Upon assuming perfect capacity achieving coding, the instantaneous data rate in the i th TS of the t th TF can be expressed as

$$R_{ti} = W \log_2 \left(1 + \frac{\alpha_t g_{ti}}{\sigma^2} p_{ti} \right), \quad (1)$$

where W is the transmission bandwidth, σ^2 is the noise power, and p_{ti} is the transmit power in the i th TS of the t th TF.

B. Video Streaming and Power Consumption Model

The video playback starts after the user has received the first video segment. To avoid stalling, each segment should be downloaded to the user's buffer before playback. We assume that the buffer capacity is higher than the video file size, which is reasonable for contemporary mobile devices. Hence, no buffer overflow is considered. Then, the following throughput constraint should be satisfied

$$\sum_{n=1}^m \sum_{t=(n-1)L_v+1}^{nL_v} \sum_{i=1}^{N_s} \tau R_{ti} \geq \sum_{n=2}^{m+1} S_n, \quad m = 1, \dots, N_v - 1, \quad (2)$$

where $\sum_{t=(n-1)L_v+1}^{nL_v} \sum_{i=1}^{N_s} \tau R_{ti}$ is the amount of data transmitted to the user during the playback of the n th segment, S_n is the size of the segment that is known after the user issues a request.

The energy consumed by a BS for video transmission during the t th TF is modeled as [26]

$$E_t = \frac{1}{\rho} \sum_{i=1}^{N_s} \tau p_{ti} + \Delta T P_c, \quad (3)$$

where ρ reflects the power-efficiency of the power amplifier, and P_c is the power dissipated by the baseband and radio frequency circuits as well as by the cooling and power supply.

To find the best power allocation among TSs that minimizes the average energy consumption subject to the throughput and maximal power constraints, the problem can be formulated as

$$\text{P1: } \min_{\{p_{ti}\}} \mathbb{E}_{\alpha_t, g} \left[\sum_{t=1}^{(N_v-1)L_v} \left(\frac{1}{\rho} \sum_{i=1}^{N_s} \tau p_{ti} + \Delta T P_c \right) \right] \quad (4a)$$

$$\text{s.t. } \sum_{n=1}^m \sum_{t=(n-1)L_v+1}^{nL_v} \sum_{i=1}^{N_s} \tau R_{ti} \geq \sum_{n=2}^{m+1} S_n, \quad m = 1, \dots, N_v - 1 \quad (4b)$$

$$p_{ti} \leq P_{\max}, \quad \forall t, i, \quad (4c)$$

where $\mathbb{E}_{\alpha_t, g}[\cdot]$ denotes the expectation taken over both the large-scale and small-scale fadings, while P_{\max} is the maximal transmit power of each BS. The distribution of α_t depends on the user's mobility pattern and R_{ti} in the throughput constraint depends on g_{ti} and α_t , all of which are unknown in advance. Without prediction, it is impossible to solve problem P1 at the beginning of video streaming. In the sequel, we resort to RL to find the solution.

III. ENERGY-SAVING POWER ALLOCATION BASED ON DDPG

In this section, we establish a RL framework for P1 and propose a policy learning algorithm.

A standard RL problem can be formulated as an MDP, where an agent learns how to achieve a goal from its interactions with the environment in a sequence of discrete time steps $t = 1, 2, \dots, T$ [15]. At each time step t , the agent observes the state \mathbf{s}_t of the environment and executes an action a_t . Then, the agent receives a reward r_t from the environment and transits into a new state \mathbf{s}_{t+1} . The interaction of the agent with the environment is then captured by an experience vector $\mathbf{e}_t = [\mathbf{s}_t, a_t, r_t, \mathbf{s}_{t+1}]$. The agent learns a policy from its experiences for minimizing an expected return, which reflects the cumulative reward received by the agent during the T -time-step episode. The policy (denoted by π) determines which action should be executed in which state. The expected return is defined as $\mathbb{E} \left[\sum_{t=1}^{T-1} \gamma^{t-1} r_t \right]$, where γ denotes the discount factor.

A. Reinforcement Learning Framework

In our learning-aided network, the MEC and cloud servers jointly serve as the agent. A direct formulation of the RL problem is to regard the instantaneous power p_{ti} allocated to the i th TS as the action. Then, the action depends on the instantaneous channel gain $\alpha_t g_{ti}$, which therefore should be included into the state. However, this incurs millisecond-level information exchange between the MEC server and each BS, which yields excessive signaling overhead. Furthermore, this makes it hard for the agent to learn a good policy, because g_{ti} is hard to predict beyond the channel's coherence time (i.e., the duration of a TS in the model considered).

In fact, g_{ti} can be regarded as a multiplicative impairment imposed on α_t and hence $\alpha_t g_{ti}$ has a much higher dynamic range than α_t . This inspires us to find the action and the state that only depend on α_t .

1) *Action*: In practice, it is not hard to evaluate the distribution of small-scale fading. Based on the distribution, we can first derive the optimal power allocation policy for each TF to minimize the average energy consumed in the TF to achieve an arbitrarily given average data rate. Then, by optimizing the average rate for each TF, we can obtain the optimal power allocation for the whole video streaming session to minimize the overall energy consumption. This suggests that we can select the average data rate of each TF as the action. In this way, the action and state for the RL agent are independent of g_{ti} .

Based on (3), the average energy consumption in the t th TF can be expressed as

$$\bar{E}_t = \mathbb{E}_g \left[\frac{1}{\rho} \sum_{i=1}^{N_s} \tau p_{ti} \right] + \Delta T P_c, \quad (5)$$

where $\mathbb{E}_g[\cdot]$ denotes the expectation taken over small-scale fading. Then, the objective function of problem P1 can be rewritten as $\mathbb{E}_{\alpha_t} \left[\sum_{t=1}^{(N_v-1)L_v} \bar{E}_t \right]$. For the t th TF, to achieve an arbitrarily given average rate \bar{R}_t , the optimal power allocation minimizing the average energy consumption in the t th TF can be found by solving the following problem,

$$\text{P2} : \forall t, \quad \min_{\{p_{ti}\}} \bar{E}_t \quad (6a)$$

$$s.t. \quad \mathbb{E}_g \left[W \log_2 \left(1 + \frac{\alpha_t}{\sigma^2} p_{ti} g_{ti} \right) \right] = \bar{R}_t \quad (6b)$$

$$0 \leq p_{ti} \leq P_{\max}, \quad \forall i, \quad (6c)$$

where $\mathbb{E}_g \left[W \log_2 \left(1 + \frac{\alpha_t}{\sigma^2} p_{ti} g_{ti} \right) \right]$ is the average data rate in the t th TF. The optimal solution of P2 is formulated in the following proposition.

Proposition 1. *The optimal power allocation policy in the t th TF is*

$$p^{\text{opt}}(\alpha_t g_{ti}; \xi_t) = \begin{cases} 0, & \alpha_t g_{ti} \leq \frac{\sigma^2}{\xi_t} \\ \xi_t - \frac{\sigma^2}{\alpha_t g_{ti}}, & \frac{\sigma^2}{\xi_t} < \alpha_t g_{ti} < \frac{\sigma^2}{\xi_t - P_{\max}} \\ P_{\max}, & \alpha_t g_{ti} \geq \frac{\sigma^2}{\xi_t - P_{\max}}, \end{cases} \quad (7)$$

where the parameter ξ_t can be obtained by solving the following equation

$$\bar{R}_t = \int_0^\infty W \log_2 \left(1 + \frac{\alpha_t}{\sigma^2} p^{\text{opt}}(\alpha_t g, \xi_t) g \right) \rho(g) dg \quad (8)$$

via bisection search, and $\rho(g)$ denotes the probability density function (PDF) of g_{ti} .

Proof: See Appendix A. ■

Let the function $\xi^{\text{opt}}(\bar{R}_t)$ denote the relationship between ξ_t and \bar{R}_t found from (8), i.e., $\xi_t \triangleq \xi^{\text{opt}}(\bar{R}_t)$, whose expression can be obtained for a special case in the following corollary.

Corollary 1. *For Rayleigh fading and a large value of P_{\max} , we have*

$$\xi^{\text{opt}}(\bar{R}_t) = \frac{\sigma^2}{\alpha_t} \left[E_1^{-1} \left(\frac{\bar{R}_t \ln 2}{W} \right) \right]^{-1}, \quad (9)$$

where $E_1^{-1}(x)$ denotes the inverse function of the exponential integral function $E_1(x) \triangleq \int_x^\infty \frac{e^{-t}}{t} dt$.

Proof: See Appendix B. ■

Since we have obtained the optimal power allocation policy in the t th TF at an arbitrarily given average data rate \bar{R}_t , the original problem P1 can be solved equivalently by first optimizing the average rate for each TF, i.e., $\{\bar{R}_t\}_{t=1, \dots, (N_v-1)L_v}$, and then obtaining the optimal power allocation for each TF using (7). Given the relationship between ξ_t and \bar{R}_t (i.e., $\xi^{\text{opt}}(\bar{R}_t)$) under the optimal power allocation policy (i.e., $p^{\text{opt}}(\alpha_t g_{ti}; \xi_t)$), the MEC server only has to decide the **action** as

$$a_t = \bar{R}_t. \quad (10)$$

Upon determining the action, the MEC server can compute ξ_t by bisection search based on (8) for the general case or by (9) for the special case given in Corollary 1, followed by sending ξ_t to the specific BS that the user is associated with. According to $p_{ti} = p^{\text{opt}}(\alpha_t g_{ti}; \xi_t)$, the BS can adjust the transmit power in each TS of the t th TF. In this way, the agent interacts with the environment on a frame-by-frame basis (i.e., the time step is set as a TF on a second-level timescale as shown in Fig. 2) and the computational load of the MEC server can be reduced, while the BS can adjust the transmit power for each TS on a millisecond-level timescale.

2) *State*: Since the average power consumed by video transmission depends on the large-scale channel gain, α_t should be included into the state. To help the agent implicitly predict the user's mobility pattern, the state should also include the channel gains in the past N_t TFs. Since different locations of a user may result in the same large-scale channel gain between the user and its associated BS, we further include the large-scale channel gains between the user and $(N_b - 1)$ adjacent BSs. Let us now define a vector $\boldsymbol{\alpha}_t \triangleq [\alpha_{1,t}, \dots, \alpha_{N_b,t}]$, where $\alpha_{n,t}$ is the large-scale channel gain between the user and the BS with the n th largest large-scale channel gain, and $\alpha_{1,t}$ is the large-scale channel gain between the user device and its associated BS (i.e., $\alpha_{1,t} = \alpha_t$). To meet the throughput requirement, the buffer status at the user should also be incorporated into the state. Let B_t denote the amount of data remaining in the user's buffer at the t th TF. The transition of B_t obeys:

$$B_{t+1} = B_t + \sum_{i=1}^{N_s} \tau R_{ti} - I(l_t = L_v) S_{n_t}, \quad (11)$$

where $\sum_{i=1}^{N_s} \tau R_{ti}$ is the amount of data transmitted during the t th TF, $l_t \in [1, L_v]$ denotes the number of TFs that the current segment S_{n_t} has been played without stalling (which reflects the playback progress of the current segment), $I(\cdot)$ is an indicator function that equals 1 if its argument is true and 0 otherwise. When $l_t = L_v$, the segment is completely played within the t th TF and the next segment should be played in the $(t + 1)$ th TF. We use n_t to denote the index of the segment played in the t th TF and hence the size of the n_t th segment is S_{n_t} . The last term $-I(l_t = L_v) S_{n_t}$ of (11) means that the n_t th segment is removed from the buffer when its playback is completed. The evolution of the playback process obeys:

$$l_{t+1} = \begin{cases} l_t, & \text{if } S_{n_{t+1}} > B_{t+1}, \text{ i.e., video stalls} \\ \text{mod}(l_t, L_v) + 1, & \text{otherwise.} \end{cases} \quad (12)$$

As shown in (11), both l_t and S_{n_t} affect the transition of B_t to B_{t+1} and hence they should be included into the state. Finally, the **state** vector is designed as

$$\mathbf{s}_t = [B_t, S_{n_t}, l_t, \boldsymbol{\alpha}_t, \boldsymbol{\alpha}_{t-1}, \dots, \boldsymbol{\alpha}_{t-N_t}]. \quad (13)$$

3) *Reward*: The **reward** for the agent is designed as

$$r_t = - \sum_{i=1}^{N_s} \tau p_{ti} - \lambda \max\{S_{n_{t+1}} - B_{t+1}, 0\}, \quad (14)$$

where $\sum_{i=1}^{N_s} \tau p_{ti}$ is the transmit energy consumed in the t th TF, while n_{t+1} is the index of the segment to be played in the next TF. The term $-\lambda \max\{S_{n_{t+1}} - B_{t+1}, 0\}$ imposes a penalty on

the reward, when the amount of data in the user's buffer is less than the size of the segment to be played (i.e., when playback stalls), λ is the penalty coefficient, and $(S_{n_{t+1}} - B_{t+1})$ increases the impact of penalty, when there is less data in the buffer.

B. Transmission Policy Based on DDPG

The state vector defined in (13) lies in the continuous space. If \mathbf{s}_t is discretized, then the number of possible states will be huge due to the combinatorial nature of the process, and the tabular-based RL (such as Q-learning [15]) encounters the curse of dimensionality. Moreover, the action \bar{R}_t also lies in the continuous space. Value-based DRL methods such as deep Q-networks (DQNs) [27] are designed for discrete action space and hence they are not suitable. DDPG [22] is designed based on the actor-critic architecture and it is able to learn a continuous policy. In contrast to other actor-critic-based RL algorithms that employ a stochastic policy gradient, DDPG employs a deterministic policy gradient so that the gradient of the policy can be estimated more efficiently [22]. Therefore, we apply DDPG for solving the RL problem.

DDPG maintains two DNNs, namely the actor network $\mu(\mathbf{s}_t; \boldsymbol{\theta}_\mu)$ and the critic network $Q(\mathbf{s}_t, a_t; \boldsymbol{\theta}_Q)$. The DNNs' architecture in our framework is shown in Fig. 3. The actor network at the MEC server specifies the current policy by deterministically mapping each state into a specific continuous action. The output of the actor network is then used for computing the parameter $\xi_t = \xi^{\text{opt}}(\bar{R}_t)$ according to Proposition 1 or Corollary 1. Upon receiving ξ_t from the MEC server, the BS controls the transmit power at each TS within the t th TF according to the policy $p^{\text{opt}}(\alpha_t g_{ti}; \xi_t)$ based on the current instantaneous channel gain $\alpha_t g_{ti}$. The critic network stored at the cloud server is used for approximating the *action-value function*, $Q_\mu(\mathbf{s}_t, a_t) \triangleq \mathbb{E} \left[\sum_{i=t}^T \gamma^{i-t} r_i \mid \mathbf{s}_t, a_t, \mu \right]$, which is the expected return achieved by policy μ , when taking action a_t under state \mathbf{s}_t .

During the interactions with the environment, the MEC server collects the experience $\mathbf{e}_t = [\mathbf{s}_t, a_t, r_t, \mathbf{s}_{t+1}]$ from the BSs in the database at the cloud server as $\mathcal{D} = \{\mathbf{e}_1, \dots, \mathbf{e}_t\}$. Every Δt TFs, a mini-batch of the experiences \mathcal{B} is sampled from \mathcal{D} to update the network parameters, representing an *experience replay* [27]. The parameters of the critic network are updated with using the batch gradient descent as

$$\boldsymbol{\theta}_Q \leftarrow \boldsymbol{\theta}_Q + \frac{\delta_Q}{|\mathcal{B}|} \nabla_{\boldsymbol{\theta}_Q} \sum_{j \in \mathcal{B}} [y_j - Q(\mathbf{s}_j, a_j; \boldsymbol{\theta}_Q)]^2, \quad (15)$$

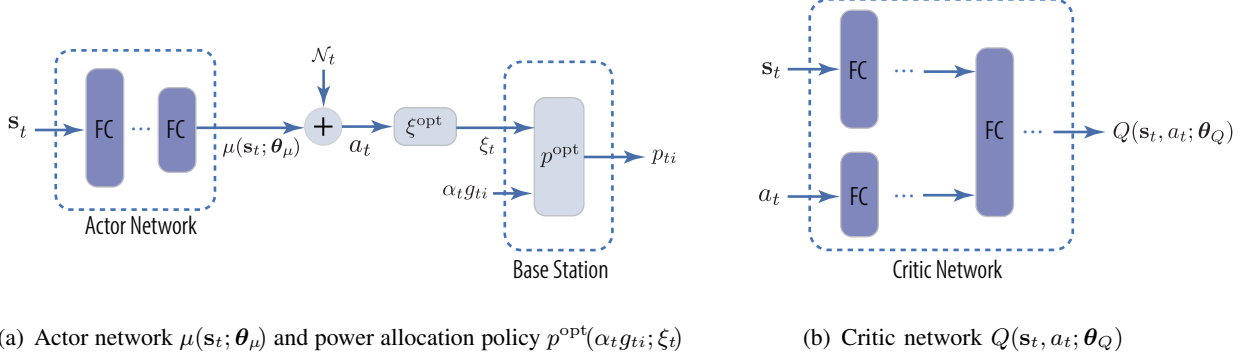


Fig. 3. Architecture of the actor and critic networks for DDPG. “FC” denotes the fully-connected layer.

where δ_Q is the learning rate of the critic network, while we have $y_j = r_j$ if all the segments have been transmitted to the user and $y_j = r_j + \gamma Q'(s_{j+1}, \mu'(s_{j+1}; \theta'_\mu); \theta'_Q)$ otherwise. Furthermore, $Q'(s, a; \theta'_Q)$ and $\mu'(s; \theta'_\mu)$ are the target critic network and target actor network, respectively, which have the same structure as $Q(\cdot)$ and $\mu(\cdot)$. They are respectively updated by $\theta'_Q \leftarrow \omega \theta_Q + (1 - \omega) \theta'_Q$ and $\theta'_\mu \leftarrow \omega \theta_\mu + (1 - \omega) \theta'_\mu$ using a very small value of ω to stabilize the learning [22].

The parameters of the actor network are updated using the sampled policy gradient as

$$\theta_\mu \leftarrow \theta_\mu + \frac{\delta_\mu}{|\mathcal{B}|} \sum_{j \in \mathcal{B}} \nabla_a Q(s_j, a; \theta_Q)|_{a=\mu(s_j; \theta_\mu)} \nabla_{\theta_\mu} \mu(s_j; \theta_\mu), \quad (16)$$

where δ_μ is the learning rate of the actor network.

To find the optimal policy, the agent has to explore the action space during the interactions with the environment. A noise term is added to the output of the actor network [22] to encourage exploration, which is formulated as $a_t = \mu(s_t; \theta_\mu) + \mathcal{N}_t$. The detailed procedure of learning the transmission policy is formulated in Algorithm 1.

IV. PDS-DDPG WITH SAFE LAYER AND VIRTUAL EXPERIENCE

In this section, we exploit the partial knowledge concerning the dynamics of the system for improving the robustness and learning efficiency of the DDPG-based energy-saving power allocation, respectively by introducing the safe layer concept into the actor network and that of the post-decision state into the critic network.

We first characterize the knowledge available concerning the state transition and the corresponding contribution to the reward in the following.

Proposition 2. *When $\tau \ll \Delta T$, we have*

$$\Pr \left(\sum_{i=1}^{N_s} \tau p_{ti} = \Delta T \bar{p}_t \right) = 1 \quad \text{and} \quad \Pr \left(\sum_{i=1}^{N_s} \tau R_{ti} = \Delta T \bar{R}_t \right) = 1, \quad (17)$$

Algorithm 1 Learning Transmission Policy Based on DDPG

```

1: Initialize critic network  $Q(s, a; \theta_Q)$  and actor network  $\mu(s; \theta_\mu)$  with random weights  $\theta_Q, \theta_\mu$ .
2: Initialize target networks  $Q'$  and  $\mu'$  with weights  $\theta'_Q \leftarrow \theta_Q, \theta'_\mu \leftarrow \theta_\mu$ .
3: Initialize replay memory  $\mathcal{D}$ ,  $\text{done} \leftarrow 0$ ,  $\text{step\_count} \leftarrow 0$ .
4: for episode = 1, 2, ... do
5:   Observe initial state  $s_1$ .
6:   for TF  $t = 1, 2, \dots$  do
7:     Select action  $a_t = \mu(s_t; \theta_\mu) + \mathcal{N}_t$ , set  $\bar{R}_t = a_t$  and  $\xi_t = \xi^{\text{opt}}(\bar{R}_t)$ .
8:     for TS  $i = 1, \dots, N_s$  do
9:       Allocate transmit power according to (7).
10:    Observe reward  $r_t$  and new state  $s_{t+1}$ .
11:    if all video segments have been transmitted to the user then
12:       $\text{done} \leftarrow 1$ 
13:    Store experience  $[s_t, a_t, r_t, s_{t+1}]$  in  $\mathcal{D}$ ,  $\text{step\_cnt} \leftarrow \text{step\_cnt} + 1$ .
14:    if  $\text{step\_cnt}$  is divisible by  $\Delta t$  then
15:      Randomly sample a mini-batch of experiences from  $\mathcal{D}$  as  $\mathcal{B} = \{[s_j, a_j, r_j, s_{j+1}]\}$ .
16:      Update the actor and critic networks according to (15) and (16), respectively.
17:      Update the target networks:  $\theta'_\mu \leftarrow \omega \theta_\mu + (1 - \omega) \theta'_\mu$ ,  $\theta'_Q \leftarrow \omega \theta_Q + (1 - \omega) \theta'_Q$ .
18:    if  $\text{done} = 1$  then
19:      break

```

where \bar{p}_t denotes the expectation of transmit power in the t th TF over the small-scale fading. Under the optimal power allocation policy, the relationship between \bar{p}_t and \bar{R}_t is

$$\bar{p}_t = \bar{p}(\bar{R}_t) = \int_{\frac{\sigma^2}{\alpha_t \xi^{\text{opt}}(\bar{R}_t)}}^{\frac{\sigma^2}{\alpha_t (\xi^{\text{opt}}(\bar{R}_t) - P_{\max})}} \left(\xi^{\text{opt}}(\bar{R}_t) - \frac{\sigma^2}{\alpha_t g_{ti}} \right) \rho(g) dg + P_{\max} \int_{\frac{\sigma^2}{\alpha_t (\xi^{\text{opt}}(\bar{R}_t) - P_{\max})}}^{\infty} \rho(g) dg. \quad (18)$$

Particularly, for Rayleigh fading and a large value of P_{\max} , we have

$$\bar{p}(\bar{R}_t) = \frac{\sigma^2}{\alpha_t} \left[e^{-E_1^{-1} \left(\frac{\bar{R}_t}{W} \ln 2 \right)} \left[E_1^{-1} \left(\frac{\bar{R}_t}{W} \ln 2 \right) \right]^{-1} - \frac{\bar{R}_t}{W} \ln 2 \right]. \quad (19)$$

Proof: See Appendix C ■

For mobile users in wireless networks, the small-scale fading gains change much faster than average channel gains, hence the condition of $\tau \ll \Delta T$ holds. Proposition 2 indicates that the energy to be consumed by the BS in the t th TF (i.e., $\sum_{i=1}^{N_s} \tau p_{ti}$) and the amount of data to be received by the user within the t th TF (i.e., $\sum_{i=1}^{N_s} \tau R_{ti}$) converge almost surely to their expectations (i.e., the ensemble-average) $\Delta T \bar{p}_t$ and $\Delta T \bar{R}_t$, respectively. Further considering (18) or (19), the sums of $\sum_{i=1}^{N_s} \tau R_{ti}$ and $\sum_{i=1}^{N_s} \tau p_{ti}$, which respectively contribute to a part of the state transition and a part of the reward as shown in (11) and (14), can be pre-computed at the beginning of TF t , given an arbitrary action \bar{R}_t .

A. Safe Layer for Actor Network

In the basic DDPG algorithm of Section III, a penalty term is added to the reward function for ensuring the throughput constraint (2). This introduces an extra hyper-parameter λ , which has to be fine-tuned for striking a tradeoff between the energy minimization against the throughput guarantee. As a result, the performance of the learned policy is sensitive to the value of λ , which has to be re-tuned for re-balancing the tradeoff, whenever the segment size changes or the user moves along a different trajectory.³ To improve the robustness of the policy, we try to meet the throughput constraint without the need for such an accurately-tuned hyper-parameter by exploiting our knowledge concerning the transitions of the user's buffer state.

According to Proposition 2, by setting the average data rate as \bar{R}_t , the amount of data to be received by the user within TF t can be pre-computed at the beginning of the TF as $\sum_{i=1}^{N_s} \tau R_{ti} = \Delta T \bar{R}_t$. Therefore, given the amount of data $\sum_{i=1}^{N_s} \tau R_{ti}$ that the user should receive within the t th TF for meeting the throughput requirement, the action in the t th frame is set as

$$\bar{R}_t = \frac{\sum_{i=1}^{N_s} \tau R_{ti}}{\Delta T}. \quad (20)$$

To guarantee the throughput constraint (2), we should ensure that the amount of data in the user's buffer cover the size of the video segment to be played. According to (11), to ensure $B_{t+1} \geq S_{n_{t+1}}$, the least amount of data that should be received by the user within the t th TF is $\sum_{i=1}^{N_s} \tau R_{ti} \geq \max\{S_{n_{t+1}} - B_t + I(l_t = L_v)S_{n_t}, 0\}$, which yields

$$\bar{R}_t \geq \frac{1}{\Delta T} \max\{S_{n_{t+1}} - B_t + I(l_t = L_v)S_{n_t}, 0\} \quad (21)$$

considering (20). To ensure that the executed action is "safe" in terms of satisfying the constraint $B_{t+1} \geq S_{n_{t+1}}$, we add an additional layer (termed as the *safe layer* [23]) to the output of the original actor network $\mu(\mathbf{s}_t; \boldsymbol{\theta}_\mu)$ to adjust the action as follows:

$$a_t = \max \left\{ \mu(\mathbf{s}_t; \boldsymbol{\theta}_\mu) + \mathcal{N}_t, \frac{1}{\Delta T} \max\{S_{n_{t+1}} - B_t + I(l_t = L_v)S_{n_t}, 0\} \right\}. \quad (22)$$

In this way, the penalty term in (14) can be removed, and hence the hyper-parameter λ is no longer needed.

³For conciseness, those simulation results are not provided.

Remark 1. Such a safe layer can also be inserted into other RL problems for satisfying the constraints, as long as the constraints can be equivalently transformed into the constraints on the action of each time step with known expressions, as exemplified by (21).⁴

B. Post-Decision State for Critic Network

General RL/DRL algorithms are applicable to the scenarios where the dynamics of the system, including the state transition probability distribution and the reward distribution, are completely unknown. However, for many problems in wireless networks, these dynamics are indeed partially known, as exemplified in Proposition 2 for the problem at hand. To exploit the knowledge available for accelerating learning, we introduce PDS to decompose the dynamics of the system into a known part and an unknown part. Specifically, PDS describes the intermediate state after the known dynamic takes place, but before the unknown dynamic takes place [24].

1) *Estimating the action-value function with the post-decision state:* Let \tilde{s}_t denote the PDS at the t th TF. For the problem considered, \tilde{s}_t is defined to characterize the buffer's state, the size of the video segment to be played, and the playback progress of the video segment after the user receives the transmitted data within the t th TF, and to characterize the large-scale channel gains before transition. To augment our exposition, we rewrite the state vector in (13) in the t th and $(t + 1)$ th TF before and after the defined PDS as follows:

$$\text{State at TF } t: \mathbf{s}_t = [B_t, S_{n_t}, l_t, \boldsymbol{\alpha}_t, \dots, \boldsymbol{\alpha}_{t-N_t}], \quad (23a)$$

$$\text{PDS at TF } t: \tilde{\mathbf{s}}_t \triangleq [B_{t+1}, S_{n_{t+1}}, l_{t+1}, \boldsymbol{\alpha}_t, \dots, \boldsymbol{\alpha}_{t-N_t}], \quad (23b)$$

$$\text{State at TF } t + 1: \mathbf{s}_{t+1} = [B_{t+1}, S_{n_{t+1}}, l_{t+1}, \boldsymbol{\alpha}_{t+1}, \dots, \boldsymbol{\alpha}_{t-N_t+1}]. \quad (23c)$$

By introducing the PDS, the reward can be decomposed into two parts formulated as $r_t = r_t^k + r_t^u$, where r_t^k is the reward received from transition $\mathbf{s}_t \rightarrow \tilde{\mathbf{s}}_t$ and r_t^u is the reward received from transition $\tilde{\mathbf{s}}_t \rightarrow \mathbf{s}_{t+1}$. Let $\rho(\mathbf{s}_{t+1}, r_t | \mathbf{s}_t, a_t)$ denote the joint conditional PDF of \mathbf{s}_{t+1} and r_t when taking action a_t at state \mathbf{s}_t , which characterizes the transition $\mathbf{s}_t \rightarrow \mathbf{s}_{t+1}$. If the transition $\tilde{\mathbf{s}}_t \rightarrow \mathbf{s}_{t+1}$ and r_t^u are independent from the action a_t (which is true for the problem considered since the transition of large-scale channel gains is independent from a_t), we can decompose the joint conditional PDF into known and unknown components as

$$\rho(\mathbf{s}_{t+1}, r_t | \mathbf{s}_t, a_t) = \iint_{(\tilde{\mathbf{s}}_t, r_t^k)} \rho^k(\tilde{\mathbf{s}}_t, r_t^k | \mathbf{s}_t, a_t) \, dr_t^k \rho^u(\mathbf{s}_{t+1}, r_t - r_t^k | \tilde{\mathbf{s}}_t) \, d\tilde{\mathbf{s}}_t, \quad (24)$$

⁴When the expressions are unknown, some approximation methods can be used as in [23].

where the conditional PDF accounting for the transition $\mathbf{s}_t \rightarrow \tilde{\mathbf{s}}_t$ (i.e., $\rho^k(\tilde{\mathbf{s}}_t, r_t^k | \mathbf{s}_t, a_t)$) is known (to be derived later), and the conditional PDF accounting for the transition $\tilde{\mathbf{s}}_t \rightarrow \mathbf{s}_{t+1}$ (i.e., $\rho^u(\mathbf{s}_{t+1}, r_t - r_t^k | \tilde{\mathbf{s}}_t)$) is unknown.

Let us define the *PDS-value function* of $\tilde{\mathbf{s}}_t$ as the expected accumulated reward achieved by policy μ started from $\tilde{\mathbf{s}}_t$, i.e., $V_\mu(\tilde{\mathbf{s}}_t) \triangleq \mathbb{E} \left[r_t^u + \sum_{i=t+1}^{T-1} \gamma^{i-t} r_i | \tilde{\mathbf{s}}_t \right]$. Then, based on the factorization of the state transition by PDS as well as on the definitions of the action-value and PDS-value functions, the relationship between the PDS-value function $V_\mu(\cdot)$ and the action-value function $Q_\mu(\cdot)$ can be expressed as

$$V_\mu(\tilde{\mathbf{s}}_t) = \iint_{(\mathbf{s}_{t+1}, r_t^u)} [r_t^u + \gamma Q_\mu(\mathbf{s}_{t+1}, \mu(\mathbf{s}_{t+1}))] \rho^u(\mathbf{s}_{t+1}, r_t^u | \tilde{\mathbf{s}}_t) dr_t^u d\mathbf{s}_{t+1}, \quad (25)$$

$$Q_\mu(\mathbf{s}_t, a_t) = \iint_{(\tilde{\mathbf{s}}_t, r_t^k)} [r_t^k + V_\mu(\tilde{\mathbf{s}}_t)] \rho^k(\tilde{\mathbf{s}}_t, r_t^k | \mathbf{s}_t, a_t) dr_t^k d\tilde{\mathbf{s}}_t. \quad (26)$$

By substituting (25) into (26) and considering $r_t = r_t^k + r_t^u$ as well as $\rho(\mathbf{s}_{t+1}, r_t | \mathbf{s}_t, a_t) = \iint_{(r_t^u, \tilde{\mathbf{s}}_t)} \rho^k(\tilde{\mathbf{s}}_t, r_t - r_t^u | \mathbf{s}_t, a_t) \rho^u(\mathbf{s}_{t+1}, r_t^u | \tilde{\mathbf{s}}_t) dr_t^u d\tilde{\mathbf{s}}_t$, we arrive at

$$Q_\mu(\mathbf{s}_t, a_t) = \iint_{(\mathbf{s}_{t+1}, r_t)} [r_t + \gamma Q_\mu(\mathbf{s}_{t+1}, \mu(\mathbf{s}_{t+1}))] \rho(\mathbf{s}_{t+1}, r_t | \mathbf{s}_t, a_t) dr_t d\mathbf{s}_{t+1}, \quad (27)$$

which is actually the Bellman equation with respect to Q_μ , based on which the critic network parameter θ_Q is updated by the DDPG. Considering that (27) can be derived from (25) and (26), we can directly develop corresponding RL algorithm based on (25) and (26) rather than (27).

Specifically, since the transition PDF $\rho^k(\tilde{\mathbf{s}}_t, r_t^k | \mathbf{s}_t, a_t)$ can be derived, the action-value function $Q_\mu(\mathbf{s}_t, a_t)$ can be obtained by estimating the PDS-value function $V_\mu(\tilde{\mathbf{s}}_t)$ in the right-hand-side (RHS) of (26). Compared to directly estimating $Q_\mu(\mathbf{s}_t, a_t)$, estimating $V_\mu(\tilde{\mathbf{s}}_t)$ is more sample-efficient, since $V_\mu(\tilde{\mathbf{s}}_t)$ does not depend on the action and hence it has a lower dimension.

2) *Deriving the conditional PDF accounting for the transition $\mathbf{s}_t \rightarrow \tilde{\mathbf{s}}_t$:* In what follows, we derive $\rho^k(\tilde{\mathbf{s}}_t, r_t^k | \mathbf{s}_t, a_t)$. In particular, we show that $\tilde{\mathbf{s}}_t$ and r_t^k become deterministic given that the agent executes action a_t at state \mathbf{s}_t . According to Proposition 2, we have $\sum_{i=1}^{N_s} \tau R_{ti} = \Delta T \bar{R}_t = \Delta T a_t$. Upon substituting this into (11), the first element of $\tilde{\mathbf{s}}_t$, i.e., the buffer state B_{t+1} , can be expressed as

$$\tilde{\mathbf{s}}_t[1] = B_{t+1} = B_t + \Delta T a_t - I(l_t = L_v) S_{n_t} = \mathbf{s}_t[1] + \Delta T a_t - I(\mathbf{s}_t[3] = L_v) \mathbf{s}_t[2] \quad (28)$$

which is deterministic, given \mathbf{s}_t and a_t . The second element of $\tilde{\mathbf{s}}_t$ is $\tilde{\mathbf{s}}_t[2] = S_{n_{t+1}}$, i.e., the size of the video segment to be played at the $(t+1)$ th TF, which is also deterministic given \mathbf{s}_t , because the size of each segment is known after the user issues the video request. The third element of

\tilde{s}_t is $\tilde{s}_t[3] = l_{t+1}$, i.e., the playback progress of the video segment to be played at $t + 1$. By substituting (28) into (12), l_{t+1} can be expressed as a deterministic function of \mathbf{s}_t and a_t as

$$f_1(\mathbf{s}_t, a_t) = \begin{cases} l_t, & \text{if } S_{n_{t+1}} > \mathbf{s}_t[1] + \Delta T a_t - I(\mathbf{s}_t[3] = L_v) \mathbf{s}_t[2] \\ \text{mod}(l_t, L_v) + 1, & \text{otherwise.} \end{cases} \quad (29)$$

The rest of the elements in \tilde{s}_t are the same as \mathbf{s}_t . Finally, \tilde{s}_t can be expressed as a function of \mathbf{s}_t and a_t as

$$\tilde{s}_t = \mathbf{f}_{\text{PDS}}(\mathbf{s}_t, a_t) = [\mathbf{s}_t[1] + \Delta T a_t - I(\mathbf{s}_t[3] = L_v) \mathbf{s}_t[2], S_{n_{t+1}}, f_1(\mathbf{s}_t, a_t), \mathbf{s}_t[4:]], \quad (30)$$

where $\mathbf{s}_t[x:]$ denotes the sliced vector containing the x th, $(x + 1)$ th element to the last element of \mathbf{s}_t .

Again, according to the definition of \tilde{s}_t , we can obtain $r_t^k = r_t$ and $r_t^u = 0$. Furthermore, considering Proposition 2, we have

$$\begin{cases} r_t^k = r_t = \sum_{i=1}^{N_s} \tau p_{ti} = \Delta T \bar{p}(a_t) \\ r_t^u = 0, \end{cases} \quad (31)$$

where both r_t^k and r_t^u are deterministic given \mathbf{s}_t and a_t . Thus, the transition PDF $\rho^k(\tilde{s}_t, r_t^k | \mathbf{s}_t, a_t)$ degenerates into

$$\rho^k(\tilde{s}_t, r_t^k | \mathbf{s}_t, a_t) = \delta(\tilde{s}_t - \mathbf{f}_{\text{PDS}}(\mathbf{s}_t, a_t), r_t^k - \Delta T \bar{p}(a_t)), \quad (32)$$

where $\delta(\tilde{s}_t - x, r_t^k - y)$ denotes the two-dimensional Dirac delta function defined as $\int_{\tilde{s}_t} \int_{r_t^k} \delta(\tilde{s}_t - x, r_t^k - y) d\tilde{s}_t dr_t^k = 1$, and $\delta(\tilde{s}_t - x, r_t^k - y) = 0$ if $\tilde{s}_t \neq x$ or $r_t^k \neq y$.

Finally, by substituting (31) and (32) into (25) and (26), we can obtain the relationship between $V_\mu(\cdot)$ and $Q_\mu(\cdot)$ for the video streaming problem considered as

$$V_\mu(\tilde{s}_t) = \gamma \int_{\mathbf{s}_{t+1}} Q_\mu(\mathbf{s}_{t+1}, \mu(\mathbf{s}_{t+1})) \rho^u(\mathbf{s}_{t+1} | \tilde{s}_t) d\mathbf{s}_{t+1} \quad (33)$$

$$Q_\mu(\mathbf{s}_t, a_t) = \Delta T \bar{p}(a_t) + V_\mu(\mathbf{f}_{\text{PDS}}(\mathbf{s}_t, a_t)). \quad (34)$$

Observe from (30) that multiple state-action pairs may lead to the same PDS.⁵ This suggests that if we directly estimate the PDS-value function on the RHS of (34), the action-value of multiple state-action pairs on the left-hand-side can be updated accordingly based on (34), which indicates the potential for accelerating the learning procedure. In Fig. 4, we summarize the relationship between \mathbf{s}_t , \tilde{s}_t and \mathbf{s}_{t+1} .

⁵For example, state $[B_t, S_{n_t}, l_t, \alpha_t, \dots, \alpha_{t-N_t}]$ and $[B_t + \Delta T x, S_{n_t}, l_t, \alpha_t, \dots, \alpha_{t-N_t}]$ transit to the same PDS if executing action a_t and $a_t - x$, respectively.

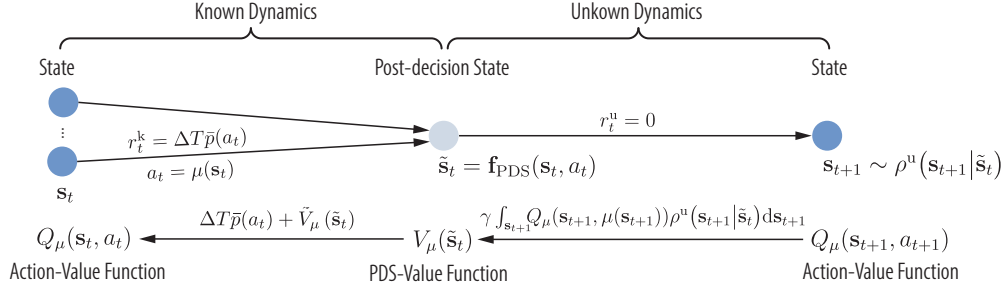


Fig. 4. The relations between states s_t , s_{t+1} and the PDS \tilde{s}_t .

3) *PDS-based DDPG algorithm:* Again, we parameterize the transmission policy μ by a DNN having the parameter θ_μ . Upon adding the safe layer defined by (22), the structure of the modified actor network $\mu_s(s_t, \mathcal{N}_t; \theta_\mu)$ is shown in Fig 5(a). Based on (34), we use a DNN $V(\tilde{s}_t; \theta_V)$ to approximate $V_\mu(\tilde{s}_t)$ and then obtain the approximated $Q_\mu(s_t, a_t)$ as

$$Q(s_t, a_t; \theta_V) = \Delta T \bar{p}(a_t) + V(\mathbf{f}_{\text{PDS}}(s_t, a_t); \theta_V), \quad (35)$$

whose structure is shown in Fig. 5(b).

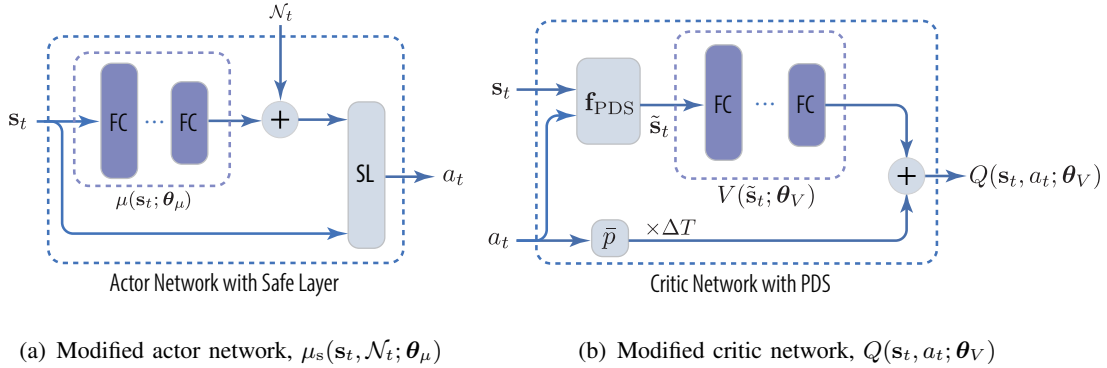


Fig. 5. Architecture of the actor and critic networks for enhanced DDPG with PDS and safe layer. “SL” denotes the safe layer. The power allocation component that takes a_t as the input is the same as in the right of Fig. 3(a), and hence is omitted here.

Upon comparing Fig. 5 and Fig. 3, we can see that by exploiting the partially known dynamics, the structures of the actor and critic networks are incorporated with the aid of known components tailored for the system considered, i.e., the safe layer (22), $\mathbf{f}_{\text{PDS}}(s_t, a_t)$ and $\Delta T \bar{p}(a_t)$, instead of only consisting of fully-connected layers having unknown parameters to be learned.

Remark 2. 1) *PDS exploits partial information about the environment so that less parameters of the critic network have to be learned.* 2) *Updating a single PDS value provides information about the value of many state-action pairs, which further accelerates the learning procedure.*

In Section V, we will show that given the modified structure, the number of nodes in the fully-connected layers can be significantly reduced, and hence the convergence can be accelerated.

Analogous to the update rule of θ_Q in (15) based on the Bellman equation (27), the update rule of θ_V for the modified critic network can be obtained based on (33) as

$$\theta_V \leftarrow \theta_V + \frac{\delta_V}{|\mathcal{B}|} \nabla_{\theta_V} \sum_{j \in \mathcal{B}} [y_j - V(\mathbf{f}_{\text{PDS}}(\mathbf{s}_j, a_j); \theta_V)]^2, \quad (36)$$

where we have substituted $\tilde{\mathbf{s}}_t = \mathbf{f}_{\text{PDS}}(\mathbf{s}_t, a_t)$, $y_j = 0$ if all the segments have been transmitted to the user, while $y_j = \gamma Q'(\mathbf{s}_{j+1}, \mu'_s(\mathbf{s}_{j+1}, 0; \theta'_\mu); \theta'_V)$ otherwise. Again, $Q'(\cdot; \theta'_V)$ and $\mu'_s(\cdot; \theta'_\mu)$ are the target critic network and target actor network, respectively, which have the same structure as $Q(\cdot; \theta_V)$ and $\mu_s(\cdot; \theta_\mu)$, and are respectively updated by $\theta'_V \leftarrow \omega \theta_V + (1 - \omega) \theta'_V$ and $\theta'_\mu \leftarrow \omega \theta_\mu + (1 - \omega) \theta'_\mu$.

From (35), we can arrive at

$$\nabla_a Q(\mathbf{s}_t, a; \theta_V) = \Delta T \nabla_a \bar{p}(a) + \nabla_{\tilde{\mathbf{s}}} V(\tilde{\mathbf{s}}; \theta_V) \Big|_{\tilde{\mathbf{s}}=\mathbf{f}_{\text{PDS}}(\mathbf{s}_t, a)} \nabla_a \mathbf{f}_{\text{PDS}}(\mathbf{s}_t, a), \quad (37)$$

By substituting (37) into (16), we can derive the update rule of θ_V for the modified actor network as

$$\theta_\mu \leftarrow \theta_\mu + \frac{\delta_\mu}{|\mathcal{B}|} \sum_{j \in \mathcal{B}} \left[\Delta T \nabla_a \bar{p}(a) + \nabla_{\tilde{\mathbf{s}}} V(\tilde{\mathbf{s}}; \theta_V) \nabla_a \mathbf{f}_{\text{PDS}}(\mathbf{s}_j, a) \right] \Big|_{a=\mu_s(\mathbf{s}_j, 0; \theta_\mu), \tilde{\mathbf{s}}=\mathbf{f}_{\text{PDS}}(\mathbf{s}_j, a)} \nabla_{\theta_\mu} \mu_s(\mathbf{s}_j, 0; \theta_\mu). \quad (38)$$

Remark 3. *The relationship between the PDS-value function and the action-value function, i.e., (25) and (26), are also applicable to other RL problems as long as: 1) Parts of the state transition are known; 2) The transition from PDS $\tilde{\mathbf{s}}_t$ to the next state \mathbf{s}_{t+1} is independent from a_t . Therefore, the proposed approach of incorporating PDS into the DRL algorithm can be extended to other RL problems.*

C. Virtual Experiences

The analysis in the previous subsection suggests that the state transition $\mathbf{s}_t[1:3] \rightarrow \mathbf{s}_{t+1}[1:3]$ and the reward can be obtained in advance, given \mathbf{s}_t and a_t . Further considering that the transition of the average channel gain does not depend on $\mathbf{s}_t[1:3]$ and a_t , we are able to generate virtual experience based on historical traces of average channel gains recorded for previously served users. The virtual experience can then be used for training the DNNs for further accelerating the learning procedure by relying on less interactions with environment.

Specifically, let $\mathbf{h}^{(j)} = [\boldsymbol{\alpha}_t^{(j)}]_{t=1-N_t, \dots, T}$ denote a trace of the average channel gains of a previously served user recorded during a video streaming episode. From $\mathbf{h}^{(j)}$ we can generate an

initial state for a virtual user as $\mathbf{s}_1 = [B_1, S_{n_1}, l_1, \boldsymbol{\alpha}_1^{(j)}, \dots, \boldsymbol{\alpha}_{1-N_t}^{(j)}]$ and obtain the action output by the actor network as $a_1 = \mu_s(\mathbf{s}_1, \mathcal{N}_1; \boldsymbol{\theta}_\mu)$. Assuming that the average channel gains of the virtual user evolve the same as recorded in the historical trace $\mathbf{h}^{(j)}$, the next state and the reward can be directly computed as $\mathbf{s}_2 = [\mathbf{f}_{\text{PDS}}(\mathbf{s}_1, a_1)[1:3], \boldsymbol{\alpha}_2^{(j)}, \dots, \boldsymbol{\alpha}_{2-N_t}^{(j)}]$ and $r_1 = \Delta T \bar{p}(a_1)$ based on (30) and (31), respectively. This suggests that the agent can deduce how the episode continues for a given transmission policy and channel trace. Hence, it can generate virtual experience accordingly, given that $\mathbf{h}^{(j)}$ is a true channel trace sampled from the same wireless environment, the virtual experiences can be used for training both the actor and the critic networks.

To generate and exploit the virtual experiences, every time a real episode terminates, we store the channel trace into the channel trace memory \mathcal{H} and randomly sample K traces from \mathcal{H} to generate K virtual episodes. The virtual experiences are stored into the experience relay memory \mathcal{D} so that the virtual experiences can be sampled together with the real experiences for training both the actor and critic networks. The whole learning procedure of PDS-DDPG using virtual experiences is shown in Algorithm 2.

Remark 4. *The way we generate virtual experiences can be extended to other RL problems, as long as the unknown dynamics are independent from the known dynamics. This is true for many problems in wireless networks, where the dynamics of wireless channel do not depend on the action and on the transition of other elements in the state.*

V. SIMULATION RESULTS

In this section, we evaluate the performance of the proposed DRL-based policies by comparing them to the benchmark policies via simulations.

A. Simulation Setup

We consider several scenarios, where users are moving along one or multiple roads across multiple cells, as shown in Fig. 6. The distance between the adjacent BSs is 500 m and the maximal transmit power of each BS is 46 dBm. The noise power is -95 dBm/Hz and the transmission bandwidth of each user is 2 MHz. Since the circuit power consumption is the same for all the policies considered, we only evaluate the transmit energy consumed by video streaming. The path loss is modeled as $35.3 + 37.6 \log_{10}(d)$ in dB where d is the distance between the user and BS in meters. The small-scale channel is Rayleigh fading. The playback duration

Algorithm 2 Transmission Policy Learning Based on PDS-DDPG with Virtual Experience

```

1: Initialize modified critic and actor networks  $Q(s, a; \theta_V)$  and  $\mu(s, \mathcal{N}; \theta_\mu)$  with random weights  $\theta_V, \theta_\mu$ .
2: Initialize target networks  $Q'$  and  $\mu'$  with weights  $\theta'_V \leftarrow \theta_V, \theta'_\mu \leftarrow \theta_\mu$ .
3: Initialize replay memory  $\mathcal{D}$ , channel trace memory  $\mathcal{H}$ ,  $\text{done} \leftarrow 0$ ,  $\text{step\_cnt} \leftarrow 0$ .
4: for episode = 1, 2, ... do
5:   Observe initial state  $s_1$  from the environment, and initialize channel trace  $\mathbf{h} \leftarrow [\alpha_{1-N_t}, \dots, \alpha_1]$ 
6:   for TF  $t = 1, 2, \dots$  do                                     # Observing real experiences
7:     Select action  $a_t = \mu(s_t, \mathcal{N}_t; \theta_\mu)$  with exploration noise, and set  $\bar{R}_t = a_t$  and  $\xi_t = \xi^{\text{opt}}(\bar{R}_t)$ .
8:     for TS  $i = 1, \dots, N_s$  do
9:       Allocate transmit power according to (7).
10:    Observe reward  $r_t$ , new state  $s_{t+1}$ , and add  $\alpha_{t+1}$  into channel trace  $\mathbf{h} \leftarrow [\mathbf{h}, \alpha_{t+1}]$ 
11:    if all video segments have been transmitted to the user then
12:       $\text{done} \leftarrow 1$ 
13:    Store  $\mathbf{e}_t = [s_t, a_t, s_{t+1}]$  in  $\mathcal{D}$ ,  $\text{step\_cnt} \leftarrow \text{step\_cnt} + 1$ 
14:    if  $\text{step\_cnt}$  is divisible by  $\Delta t$  then
15:      Randomly sample a batch from  $\mathcal{D}$ , update the actor and critic networks according to (38) and (36).
16:      Update the target networks  $\theta'_\mu \leftarrow \omega \theta_\mu + (1 - \omega) \theta'_\mu, \theta'_Q \leftarrow \omega \theta_Q + (1 - \omega) \theta'_Q$ 
17:    if  $\text{done} = 1$  then
18:      Store channel trace  $\mathbf{h}$  in  $\mathcal{H}$ 
19:       $\text{done} = 0$  and break
20:    for  $k = 1, \dots, K$  do                                     # Generating virtual experiences
21:      Randomly sample a channel trace  $\mathbf{h}^{(j)}$  from  $\mathcal{H}$  and generate initial state  $s_1$ .
22:      for  $t = 1, 2, \dots$  do
23:        Select action  $a_t = \mu(s_t, \mathcal{N}_t; \theta_\mu)$  with exploration noise.
24:        Obtain  $\alpha_{t+1}$  from  $\mathbf{h}^{(j)}$ , and obtain next state  $s_{t+1} = [\mathbf{f}_{\text{PDS}}(s_t, a_t)[1:3], \alpha_{t+1}^{(j)}, \dots, \alpha_{t-N_t+1}^{(j)}]$ 
25:        if all video segments have been transmitted to the virtual user then
26:           $\text{done} \leftarrow 1$ 
27:        Store  $\mathbf{e}_t = [s_t, a_t, s_{t+1}]$  in  $\mathcal{D}$ ,  $\text{step\_cnt} \leftarrow \text{step\_cnt} + 1$ 
28:        Repeat steps 14~16.
29:        if  $\text{done} = 1$  then
30:           $\text{done} = 0$  and break

```

of each video file is 150 s and that of each segment is 10 s. Each video segment has a size of 1 MByte. The duration of each TF is $\Delta T = 1$ s and the duration of each TS is $\tau = 1$ ms.

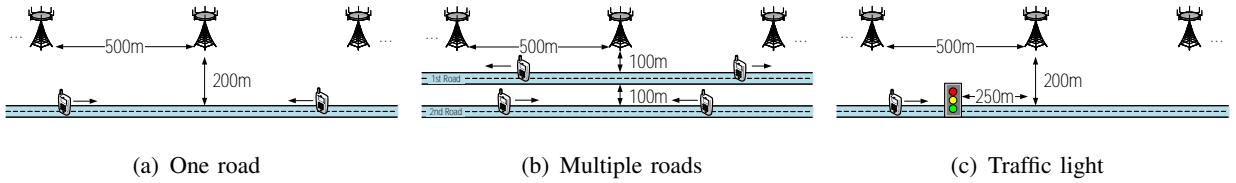


Fig. 6. Simulation scenarios.

B. Fine-Tuned Parameters in Algorithm 1 and Algorithm 2

The DNNs in our algorithms are tuned to achieve the best performance, which are as follows:

- 1) Algorithm 1: For the actor network, $\mu(\cdot)$ has four fully-connected layers each with 600 nodes. For the critic network, the state and action first go through three fully-connected

layers each having 600 nodes and a single fully-connected layer having 600 nodes, which are then concatenated, followed by two fully-connected layers each having 600 nodes.

- 2) Algorithm 2: For the modified actor and critic networks, both $\mu(\cdot)$ and $V(\cdot)$ have three fully-connected layers, each with 200 nodes. Based on these numbers of layers and nodes, the total number of unknown parameters to be learned in the modified networks is reduced roughly by a factor of 10 compared to the original actor and critic networks of Algorithm 1. This indicates the potential of employing PDS and the safe layer in improving the convergence speed and reducing the computational complexity.

All the hidden layers of the above DNNs use the rectified linear units (ReLU) as the activation function. The output layer of the critic and modified critic networks has no activation function. The network $\mu(\cdot)$ of both the actor and the modified actor networks employs $0.5 \times [\tanh(x) + 1]$ as the activation function, which normalizes the output within $[0, 1]$. For the state representation, we set $N_b = 2$ and $N_t = 2$. Since the elements of the input have different ranges and units, we normalize the large-scale channel gain as $45 + \log_2(\alpha_{b,t})$ before going through the DNNs and employ batch normalization [28] for each fully-connected layer.

The Adam method of [29] is used for adjusting the learning rate during training, and the initial learning rate is $\delta_\mu = 10^{-3}$, $\delta_Q = \delta_V = 10^{-4}$. The update rate for the target networks is $\omega = 2.5 \times 10^{-3}$. We also add a L_2 -norm regularization term with weight 10^{-3} on the loss function when training the critic network to avoid over-fitting. The mini-batch size for gradient descent is $|\mathcal{B}| = 128$. The update interval is set to $\Delta t = 4$. The discount factor is set to $\gamma = 1$ and the penalty coefficient for Algorithm 1 is set as $\lambda = 30$, respectively. The noise term n_t obeys the Gaussian distribution with zero mean and a variance reduced linearly from 0.1 to zero during the training phase and remains zero during the testing phase.

C. Performance Evaluation

We compare the proposed DRL-based policies to the following baselines:

- *Predict & Optimize*: This is the existing first-predict-then-optimize PRA policy, which first predicts the future average channel gains within a prediction window, and then determines the target average data rate \bar{R}_t for each frame based on the predicted average channel gains for minimizing the accumulated energy consumption [11]. When the future average channel gains are perfect, this policy can serve as the performance upper bound (and hence called “optimal policy” in the sequel). To obtain the predicted average channel gains, we train

a fully connected DNN for predicting the user locations and compute the future average channel gains based on the path loss model.

- *Non-predictive*: This is the existing power allocation policy operating without exploiting any future information. To satisfy the throughput constraint, the BS maintains the average data rate as $\bar{R}_t = S_{n_{t+1}}/L_v$ so that the segment to be played in the next TF is downloaded in the current TF. Without using the predicted information, this policy can only minimize the average energy consumption in the current TF via the power allocation given by (7).

In what follows, we compare the performance of the policies in different scenarios.

1) *Same Road & Constant Speed*: We first consider the scenario shown in Fig. 6(a), where each user moves along the same road at a constant velocity of 16 m/s. In this case, a well-trained DNN can perfectly predict the future locations of users and hence “*Predict & Optimize*” can achieve the optimal performance (with legend “*Optimal*”).

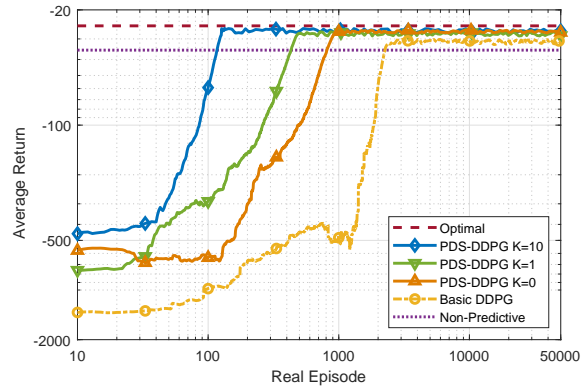


Fig. 7. Impact of the safe layer, post-decision state and virtual experience on the learning curves, K is the number of virtual episodes. The results are averaged over 30 Monte Carlo trials with random initial user locations and over 300 successive episodes.

In Fig. 7, we show the learning curves of the proposed DRL-based policies. Considering that the major concern of RL convergence speed lies in the number of interactions between the agent and the environment, the x -axis represents the number of real episodes. Since there is no video stalling after convergence (and hence no penalty on the reward), the minus value of the converged return is the accumulated transmit energy consumption. We can see that the proposed DRL-based policies converge to the optimal policy and they outperform “*Non-predictive*” after convergence. By exploiting our knowledge concerning the system dynamics, PDS-DDPG (i.e., Algorithm 2) outperforms the basic DDPG (i.e., Algorithm 1) both in terms of the convergence speed and the average return achieved. Specifically, by employing PDS and the safe layer, “*PDS-DDPG*

$K = 0$ ” converges 2.5 times faster than “*Basic DDPG*”. By further training using both the real and virtual experiences with $K = 1$ and $K = 10$, “*PDS-DDPG $K = 1$* ” and “*PDS-DDPG $K = 10$* ” convergence five times and 20 times faster than “*Basic DDPG*”, respectively.

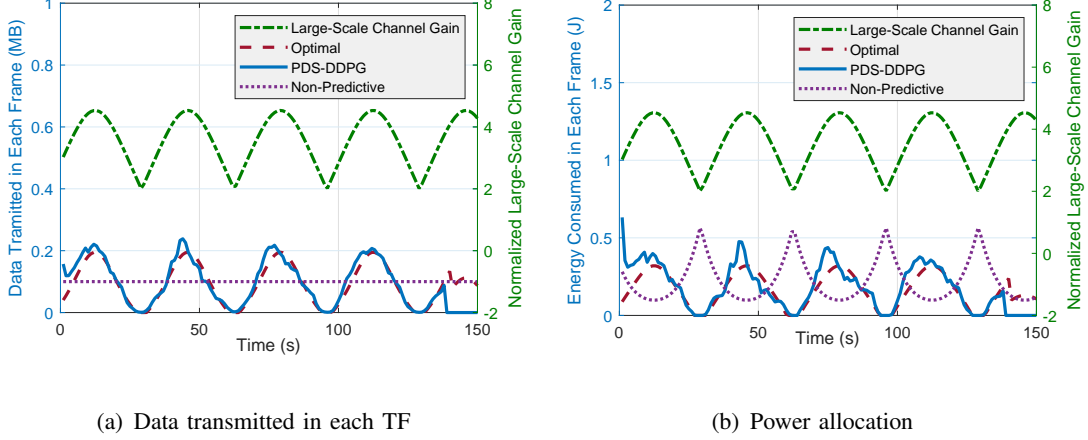
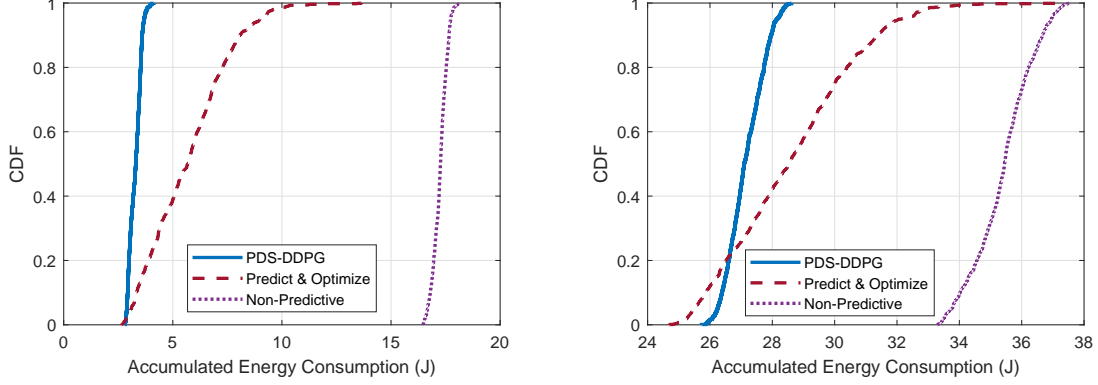


Fig. 8. Policy behavior comparison when users move along the same road with constant velocity, $K = 10$.

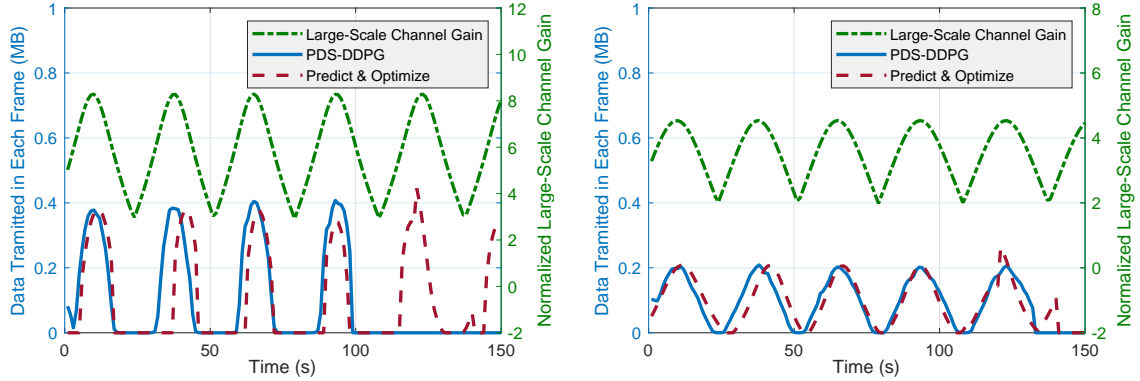
In Fig. 8, we compare how the proposed policy and the baseline policies behave over time. The result is obtained from an episode after Algorithm 2 has converged. Observe from 8(a) that the large-scale channel gains vary periodically due to the change of user-to-BS distance as the user moves along the road. The non-predictive policy has to maintain a constant average data rate for satisfying the throughput constraint, since no future information is exploited. By contrast, the DRL-based policy transmits more data when the large-scale channel gain is higher in order to save energy and behaves similarly to the optimal policy. In Fig. 8(b), we compare the energy consumptions of different policies. To maintain a constant average data rate, the non-predictive policy has to increase the transmit power in order to compensate the decrease of large-scale channel gain, which results in higher accumulated energy consumption. By contrast, the DRL-based policy and the optimal policy allocate less power when the large-scale channel gain decreases, because more data have been transmitted to the user’s buffer in advance when the large-scale channel gains are higher.

2) *Multiple Road & Random Acceleration*: To show the applicability of the DRL-based policy in more complex scenarios, we consider the scenario of Fig. 6(b), where the initial location of each user is randomly chosen from two roads at different distances from the BSs, and the users travel with random acceleration. The initial velocity of each user is 16 m/s and each user’s acceleration in each TF is drawn from the Gaussian distribution with zero mean and standard deviation of 0.1 m/s². The legitimate velocity of each user is restricted to 12 m/s \sim 20 m/s. For

“*Predict & Optimize*”, a longer prediction window (say 150 s, the same as the duration of video playback) incurs larger prediction error, which degrades the gain of PRA. For a fair comparison, the prediction window of “*Predict & Optimize*” is set to 60 s.



(a) CDF of accumulated energy consumption, the 1st road. (b) CDF of accumulated energy consumption, the 2nd road.



(c) Policy behavior, the 1st road.

(d) Policy behavior, the 2nd road.

Fig. 9. Performance and policy behavior comparison when users move along multiple roads with random acceleration. “PDS-DDPG” is trained for 3500 episodes with batch size 512, $K = 10$.

In Fig. 9, we compare the performance and the policy behavior. Observe from Fig. 9(a) and 9(b) that the DRL-based policy achieves lower accumulated energy consumption than “*Predict & Optimize*” on both roads. Moreover, the CDF curve of the DRL-based policy is steeper than that of “*Predict & Optimize*”, which suggests that the proposed policy is less sensitive to random user behavior. This is because the pre-determined average data rate of “*Predict & Optimize*” cannot promptly adapt to the real evolution of large-scale channel gains due to the user’s random acceleration, as shown in Fig. 9(c) and 9(d). By contrast, “PDS-DDPG” learns a policy that can adjust the average data rate on-line in order to adapt to the channel variation for both roads.

Upon comparing Fig. 9(a) and 9(b), we can see that the gain of “*PDS-DDPG*” over “*Predict & Optimize*” is higher when the user is moving along the 1st road. This because the 1st road is closer to the BSs and hence the channel variation is more significant along the user trajectory. Consequently, “*Predict & Optimize*” is more sensitive to the prediction errors.

3) *Random Stop*: Let us now consider the scenario of Fig. 6(c), where the users may encounter a traffic light on the road. In this scenario, the initial locations of users are uniformly distributed along the road and they may stop for $0 \sim 60$ s upon encountering a red traffic light. Since the instant of when and the duration of how long the user stops for are random, it is much harder to predict the future locations of a user for a minute-level prediction window.

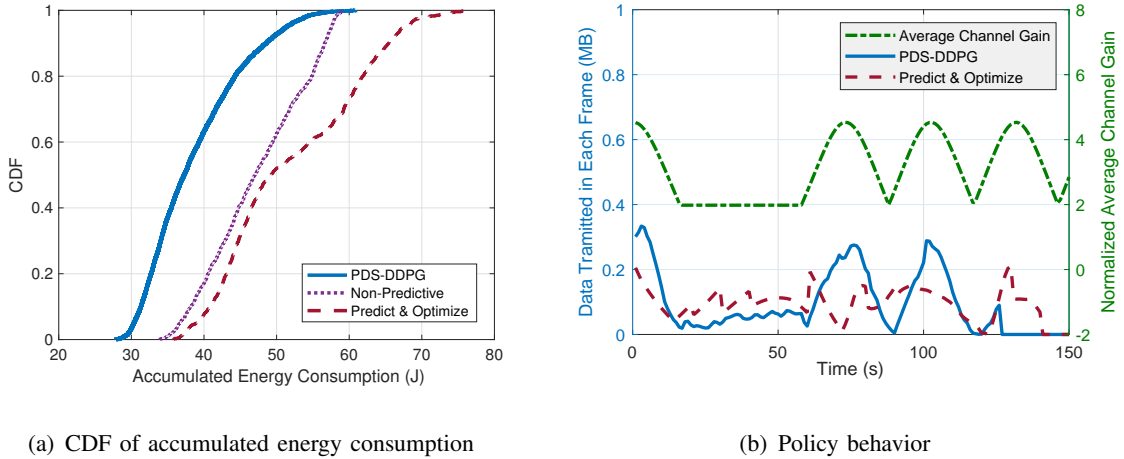


Fig. 10. Performance and policy behavior comparison when users may stop with a random duration. “*PDS-DDPG*” is trained for 2000 episodes with batch size 256, $K = 10$.

In Fig. 10, we compare the performance and behavior of the proposed policy to that of the baseline policies. We can see from Fig. 10(a) that “*Predict & Optimize*” consumes even more energy than “*Non-Predictive*”, which is due to large prediction errors caused by the random stop, as shown in Fig. 10(b). By contrast, “*PDS-DDPG*” can still learn a good policy to adapt to the channel variation.

VI. CONCLUSIONS

In this paper, we proposed a DRL-based policy for optimizing predictive power allocation for video streaming over mobile networks aimed at minimizing the average energy consumption under the throughput constraint. We formulated the problem in a RL framework and resorted to DDPG to learn the policy. To reduce the signaling overhead between the MEC server and

each BS, we judiciously designed the action and the state by exploiting the knowledge of small-scale fading distribution. To improve the robustness and accelerate learning, we integrated the concepts of safer layer, post-decision state, and virtual experience into the basic DDPG algorithm by exploiting the partially known dynamics of the system. We have also shown when those accelerating techniques can be extended to other RL problems. Our simulation results have shown that the proposed policy can converge to the optimal policy derived based on perfect future large-scale channel gains. When prediction errors exist, the proposed policy outperforms the *first-predict-then-optimize policy*. By exploiting the partial knowledge on the dynamics, the convergence speed can be dramatically improved.

APPENDIX A: PROOF OF PROPOSITION 1

Since the large-scale channel gain remains constant within a TF and the power allocation policy within a TF should adapt to the small-scale fading, p_{ti} can be expressed as a function of g_{ti} as $p_{ti} = p(g_{ti})$. Considering that g_{ti} is i.i.d. among TSs, (5) can be rewritten as

$$\bar{E}_t = \mathbb{E}_{g_{ti}} \left[\sum_{i=1}^{N_s} \tau p(g_{ti}) \right] + \Delta T P_c = \Delta T (\mathbb{E}_{g_{ti}} [p(g_{ti})] + P_c), \quad (39)$$

Since the second term P_c in (39) does not depend on the power allocation $p(g_{ti})$, problem P2 is equivalent to the following problem,

$$\text{P3 : } \forall t, \quad \min_{p(g_{ti})} \mathbb{E} [p(g_{ti})] \quad (40a)$$

$$\text{s.t. } \mathbb{E}_{g_{ti}} \left[W \log_2 \left(1 + \frac{\alpha_t}{\sigma^2} p(g_{ti}) g_{ti} \right) \right] = \bar{R}_t \quad (40b)$$

$$0 \leq p(g_{ti}) \leq P_{\max}, \quad \forall g_{ti}, \quad (40c)$$

The Lagrangian function of problem P3 can be expressed as

$$\begin{aligned} \mathcal{L}(p(g_{ti}), \lambda_1(g_{ti}), \lambda_2(g_{ti}), \mu_t) = \\ \mathbb{E}_{g_{ti}} \left[p(g_{ti}) - \lambda_1(g_{ti}) p(g_{ti}) + \lambda_2(g_{ti}) (p(g_{ti}) - P_{\max}) + \mu_t (\bar{R}_t - W \log_2 (1 + \frac{\alpha_t}{\sigma^2} p(g_{ti}) g_{ti})) \right], \end{aligned} \quad (41)$$

where $\lambda_1(g_{ti}), \lambda_2(g_{ti})$ and μ_t are the multipliers associated with the inequality and equality constraints, respectively. The Karush-Kuhn-Tucker (KKT) conditions of problem P3 are:

$$\frac{\partial \mathcal{L}}{\partial p(g_{ti})} = \mathbb{E}_{g_{ti}} \left[1 - \lambda_1(g_{ti}) + \lambda_2(g_{ti}) - \frac{\xi_t}{\sigma^2 (\alpha_t g_{ti})^{-1} + p(g_{ti})} \right] = 0 \quad (42a)$$

$$\lambda_1(g_{ti}) p(g_{ti}) = 0, \quad \forall g_{ti} \quad (42b)$$

$$\lambda_2(g_{ti})(p(g_{ti}) - P_{\max}) = 0, \quad \forall g_{ti} \quad (42c)$$

$$(40b), (40c), \lambda_1(g_{ti}) \geq 0, \lambda_2(g_{ti}) \geq 0, \quad \forall g_{ti} \quad (42d)$$

where $\xi_t = \frac{\mu_t W}{\ln 2}$. The stationary condition (42a) can be simplified to

$$1 - \lambda_1(g_{ti}) + \lambda_2(g_{ti}) - \frac{\xi_t}{\sigma^2(\alpha_t g_{ti})^{-1} + p(g_{ti})} = 0, \quad (43)$$

We first prove $\xi_t > 0$. Assuming that $\xi_t \leq 0$, we can obtain $\lambda_1(g_{ti}) \geq 1 + \lambda_2(g_{ti})$ according to (43). Then, since $\lambda_2(g_{ti}) \geq 0$, we have $\lambda_1(g_{ti}) \geq 0$. Based on (42b), we have $p(g_{ti}) = 0, \forall g_{ti}$, which contradicts to (40b). Therefore, we have $\xi_t > 0$.

When $g_{ti} < \frac{\sigma^2}{\alpha_t \xi_t}$, we have $1 - \frac{\xi_t}{\sigma^2(\alpha_t g_{ti})^{-1} + p(g_{ti})} > 0$. In this case, according to (43), we can obtain $\lambda_1(g_{ti}) > \lambda_2(g_{ti})$. Further considering that $\lambda_2(g_{ti}) \geq 0$, we have $\lambda_1(g_{ti}) > 0$. Then, according to (42b), we obtain $p(g_{ti}) = 0$. When $g_{ti} = \frac{\sigma^2}{\alpha_t \xi_t}$, we have $1 - \frac{\xi_t}{\sigma^2(\alpha_t g_{ti})^{-1} + p(g_{ti})} > 0$ if $p(g_{ti}) > 0$. However, from $1 - \frac{\xi_t}{\sigma^2(\alpha_t g_{ti})^{-1} + p(g_{ti})} > 0$, we can obtain $p(g_{ti}) = 0$ again based on (43) and $\lambda_2(g_{ti}) \geq 0$, which contradicts to $p(g_{ti}) > 0$. Therefore, we have $p(g_{ti}) = 0$.

When $g_{ti} > \frac{\sigma^2}{\alpha_t(\xi_t - P_{\max})}$, we have $1 - \frac{\xi_t}{\sigma^2(\alpha_t g_{ti})^{-1} + p(g_{ti})} < 0$. In this case, according to (43), we can obtain $\lambda_2(g_{ti}) > \lambda_1(g_{ti})$. Further considering $\lambda_1(g_{ti}) \geq 0$, we have $\lambda_2(g_{ti}) > 0$. Then, according to (42c), we can obtain $p(g_{ti}) = P_{\max}$. When $g_{ti} = \frac{\sigma^2}{\alpha_t(\xi_t - P_{\max})}$, we have $1 - \frac{\xi_t}{\sigma^2(\alpha_t g_{ti})^{-1} + p(g_{ti})} < 0$ if $p(g_{ti}) < P_{\max}$. However, from $1 - \frac{\xi_t}{\sigma^2(\alpha_t g_{ti})^{-1} + p(g_{ti})} < 0$ we can obtain $p(g_{ti}) = P_{\max}$ again based on (43) and $\lambda_1(g_{ti}) \geq 0$, which contradicts to $p(g_{ti}) < P_{\max}$. Therefore, $p(g_{ti}) = P_{\max}$.

When $\frac{\sigma^2}{\alpha_t \xi_t} < g_{ti} < \frac{\sigma^2}{\alpha_t(\xi_t - P_{\max})}$, we have $\frac{\sigma^2}{\alpha_t g_{ti}} < \xi_t < \frac{\sigma^2}{\alpha_t g_{ti}} + P_{\max}$. In this case, if $p(g_{ti}) = 0$, according to (43), we can obtain $\lambda_2(g_{ti}) > \lambda_1(g_{ti})$. Further considering that $\lambda_1(g_{ti}) \geq 0$, we have $\lambda_2(g_{ti}) > 0$. Then, according to (42c), we have $p(g_{ti}) = P_{\max}$, which contradict to $p(g_{ti}) = 0$ and hence $p(g_{ti}) > 0$. Similarity, if $p(g_{ti}) = P_{\max}$, according to (43), we can obtain $\lambda_1(g_{ti}) > \lambda_2(g_{ti})$. Further considering that $\lambda_2(g_{ti}) \geq 0$, we have $\lambda_1(g_{ti}) > 0$. Then, according to (42b), we have $p(g_{ti}) = 0$, which contradict to $p(g_{ti}) = P_{\max}$. Hence, $p(g_{ti}) < P_{\max}$. Therefore, we have $0 < p_{g_{ti}} < P_{\max}$. Consequently, we can obtain $\lambda_1(g_{ti}) = \lambda_2(g_{ti}) = 0$. By substituting $\lambda_1(g_{ti}) = \lambda_2(g_{ti}) = 0$ into (43), we have $p(g_{ti}) = \xi_t - \frac{\sigma^2}{\alpha_t g_{ti}}$.

Finally, by summarizing the above results and further considering the average rate constraint (40b), Proposition 1 has been proved. \square

APPENDIX B: PROOF OF COROLLARY 1

For Rayleigh fading, we have $\rho(g) = e^{-g}$. When P_{\max} is sufficiently high for the maximal transmit power constraints to be neglected, the optimal power allocation degenerates into

$$p^{\text{opt}}(g_{ti}; \alpha_t, \xi_t) = \begin{cases} 0, & g_{ti} \leq \frac{\sigma^2}{\alpha_t \xi_t} \\ \xi_t - \frac{\sigma^2}{\alpha_t g_{ti}}, & g_{ti} > \frac{\sigma^2}{\alpha_t \xi_t}, \end{cases} \quad (44)$$

Then, (8) degenerates into $\bar{R}_t = W \int_{\frac{\sigma^2}{\alpha_t \xi_t}}^{\infty} \log_2 \left(\frac{\alpha_t \xi_t}{\sigma^2} g \right) e^{-g} dg = \frac{W}{\ln 2} \text{E}_1 \left(\frac{\sigma^2}{\alpha_t \xi_t} \right)$, from which Corollary 1 can be proved. \square

APPENDIX C: PROOF OF PROPOSITION 2

Upon considering that $\Delta T = N_s \tau$, we obtain $\sum_{i=1}^{N_s} \tau p_{ti} = \sum_{i=1}^{N_s} \frac{\Delta T}{N_s} p_{ti} = \Delta T \sum_{i=1}^{N_s} \frac{p_{ti}}{N_s}$. When $\tau \ll \Delta T$, we have $N_s = \frac{\Delta T}{\tau} \rightarrow \infty$. Since p_{ti} is a function of g_{ti} , which is i.i.d. among TSs, we can apply the law of large numbers to obtain $\sum_{i=1}^{N_s} \frac{p_{ti}}{N_s} \xrightarrow{a.s.} \bar{p}_t$ and hence $\Pr(\sum_{i=1}^{N_s} \tau p_{ti} = \Delta T \bar{p}_t) = 1$. Similarity, we can obtain $\Pr(\sum_{i=1}^{N_s} \tau R_{ti} = \Delta T \bar{R}_t) = 1$. The average transmit power $\bar{p}_t = \int_0^{\infty} p^{\text{opt}}(g; \alpha_t, \xi_t^{\text{opt}}(\bar{R}_t)) \rho(g) dg$ can be derived from Proposition 1. Specifically, for Rayleigh fading and large transmit power, \bar{p}_t can be expressed as

$$\bar{p}_t = \int_{\frac{\sigma^2}{\alpha_t \xi_t^{\text{opt}}(\bar{R}_t)}}^{\infty} \left(\xi_t^{\text{opt}}(\bar{R}_t) - \frac{\sigma^2}{\alpha_t g} \right) e^{-g} dg = \xi_t^{\text{opt}}(\bar{R}_t) e^{-\frac{\sigma^2}{\alpha_t \xi_t^{\text{opt}}(\bar{R}_t)}} - \frac{\sigma^2}{\alpha_t} \text{E}_1 \left(\frac{\sigma^2}{\alpha_t \xi_t^{\text{opt}}(\bar{R}_t)} \right). \quad (45)$$

By substituting (9) into (45), Proposition 2 has been proved. \square

REFERENCES

- [1] D. Liu, J. Zhao, and C. Yang, "Energy-saving predictive video streaming with deep reinforcement learning," in *Proc. Globecom*, Waikoloa, USA, 2019, pp. 1–6.
- [2] Cisco, "Global mobile data traffic forecast update, 2016–2021 white paper," Feb. 2017.
- [3] L. Hanzo, P. Cherriman, and J. Streit, *Video compression and communications: from basics to H. 261, H. 263, H. 264, MPEG4 for DVB and HSDPA-style adaptive turbo-transceivers*. John Wiley & Sons, 2007.
- [4] J. Yang, P. Si, Z. Wang, X. Jiang, and L. Hanzo, "Dynamic resource allocation and layer selection for scalable video streaming in femtocell networks: A twin-time-scale approach," *IEEE Trans. on Commun.*, vol. 66, no. 8, pp. 3455–3470, Aug. 2018.
- [5] M. Choi, A. No, M. Ji, and J. Kim, "Markov decision policies for dynamic video delivery in wireless caching networks," *IEEE Trans. Wireless Commun.*, vol. 18, no. 12, pp. 5705–5718, Dec. 2019.
- [6] W. Zhang, Y. Liu, T. Liu, and C. Yang, "Trajectory prediction with recurrent neural networks for predictive resource allocation," in *Proc. IEEE ICSP*, Beijing, China, 2018, pp. 634–639.
- [7] M. Kasparick, R. L. Cavalcante, S. Valentin, S. Stańczak, and M. Yukawa, "Kernel-based adaptive online reconstruction of coverage maps with side information," *IEEE Trans. Veh. Technol.*, vol. 65, no. 7, pp. 5461–5473, Jul. 2015.
- [8] D. Tsilimantos, A. Nogales-Gómez, and S. Valentin, "Anticipatory radio resource management for mobile video streaming with linear programming," in *Proc. IEEE ICC*, Kuala Lumpur, Malaysia, 2016, pp. 1–6.

- [9] H. Abou-Zeid, H. S. Hassanein, and S. Valentin, "Energy-efficient adaptive video transmission: Exploiting rate predictions in wireless networks," *IEEE Trans. Veh. Technol.*, vol. 63, no. 5, pp. 2013–2026, Jun. 2014.
- [10] R. Atawia, H. S. Hassanein, H. Abou-Zeid, and A. Noureldin, "Robust content delivery and uncertainty tracking in predictive wireless networks," *IEEE Trans. Wireless Commun.*, vol. 16, no. 4, pp. 2327–2339, Apr. 2017.
- [11] C. She and C. Yang, "Context aware energy efficient optimization for video on-demand service over wireless networks," in *Proc. IEEE/CIC ICC, Shenzhen, China*, 2015, pp. 1–6.
- [12] N. Bui and J. Widmer, "Data-driven evaluation of anticipatory networking in LTE networks," *IEEE Trans. on Mobile Comput.*, vol. 17, no. 10, pp. 2252–2265, Oct. 2018.
- [13] J. Guo, C. Yang, and C.-L. I, "Exploiting future radio resources with end-to-end prediction by deep learning," *IEEE Access*, vol. 6, Dec. 2018.
- [14] C. She and C. Yang, "Energy efficient resource allocation for hybrid services with future channel gains," *IEEE Trans. Green Commun. and Netw.*, early access, 2019.
- [15] R. S. Sutton and A. G. Barto, *Reinforcement learning: An introduction*. MIT press Cambridge, 1998.
- [16] Y. LeCun, Y. Bengio, and G. Hinton, "Deep learning," *Nature*, vol. 521, no. 7553, pp. 436–444, 2015.
- [17] Y. C. Hu, M. Patel, D. Sabella, N. Sprecher, and V. Young, "Mobile edge computing: A key technology towards 5G," *ETSI white paper*, vol. 11, no. 11, pp. 1–16, 2015.
- [18] N. C. Luong, D. T. Hoang, S. Gong, D. Niyato, P. Wang, Y. Liang, and D. I. Kim, "Applications of deep reinforcement learning in communications and networking: A survey," *IEEE Commun. Surveys Tuts.*, vol. 21, no. 4, pp. 3133–3174, Fourthquarter 2019.
- [19] N. Zhao, Y. Liang, D. Niyato, Y. Pei, M. Wu, and Y. Jiang, "Deep reinforcement learning for user association and resource allocation in heterogeneous cellular networks," *IEEE Trans. Wireless Commun.*, vol. 18, no. 11, pp. 5141–5152, Nov. 2019.
- [20] Z. Zhang, Y. Yang, M. Hua, C. Li, Y. Huang, and L. Yang, "Proactive caching for vehicular multi-view 3D video streaming via deep reinforcement learning," *IEEE Trans. Wireless Commun.*, vol. 18, no. 5, pp. 2693–2706, May 2019.
- [21] D. Liu and C. Yang, "A deep reinforcement learning approach to proactive content pushing and recommendation for mobile users," *IEEE Access*, vol. 7, pp. 83 120–83 136, 2019.
- [22] T. P. Lillicrap, J. J. Hunt, A. Pritzel, N. Heess, T. Erez, Y. Tassa, D. Silver, and D. Wierstra, "Continuous control with deep reinforcement learning," in *Proc. ICLR*, San Diego, USA, 2015, pp. 1–14.
- [23] G. Dalal, K. Dvijotham, M. Vecerik, T. Hester, C. Paduraru, and Y. Tassa, "Safe exploration in continuous action spaces," *arXiv preprint*, 2018. [Online]. Available: <http://arxiv.org/abs/1801.08757>
- [24] N. Mastronarde and M. van der Schaar, "Fast reinforcement learning for energy-efficient wireless communication," *IEEE Trans. Signal Process.*, vol. 59, no. 12, pp. 6262–6266, Dec. 2011.
- [25] F. D. Calabrese, L. Wang, E. Ghadimi, G. Peters, L. Hanzo, and P. Soldati, "Learning radio resource management in RANs: Framework, opportunities, and challenges," *IEEE Commun. Mag.*, vol. 56, no. 9, pp. 138–145, Sept. 2018.
- [26] G. Auer, V. Giannini, C. Desset, I. Godor, P. Skillermark, M. Olsson, M. A. Imran, D. Sabella, M. J. Gonzalez, O. Blume, and A. Fehske, "How much energy is needed to run a wireless network?" *IEEE Wireless Commun.*, vol. 18, no. 5, pp. 40–49, Oct. 2011.
- [27] V. Mnih, K. Kavukcuoglu, D. Silver *et al.*, "Human-level control through deep reinforcement learning," *Nature*, vol. 518, no. 7540, p. 529, Feb. 2015.
- [28] S. Ioffe and C. Szegedy, "Batch normalization: Accelerating deep network training by reducing internal covariate shift," in *Proc. ICML*, Lille, France, 2015, pp. 448–456.
- [29] D. P. Kingma and J. Ba, "Adam: A method for stochastic optimization," in *Proc. ICLR*, Banff, Canada, 2014, pp. 1–15.